Topics in Catalysis (2021) 64:446–455
https://doi.org/10.1007/s11244-021-01414-3

ORIGINAL PAPER

Effect of Au Addition on the Catalytic Performance of CuO/CeO_2 Catalysts for CO_2 Hydrogenation to Methanol

Weiwei Wang[1] · Desiree Wager Kimpouni Tongo[1] · Lixin Song[1] · Zhenping Qu[1]

Accepted: 30 January 2021 / Published online: 18 February 2021

Abstract

The bimetallic x wt% Au–CuO/CeO_2 catalysts with different Au contents (x = 0.5, 1, 2 wt%) and Au/CeO_2, CuO/CeO_2 samples are applied for CO_2 hydrogenation to methanol. The catalysts are characterized by techniques such as XRD, Raman, XPS, H_2-TPR and CO_2-TPD measurements. It is shown that addition of 1 wt% of Au to CuO/CeO_2 improves more significantly the catalyst activity in CO_2 hydrogenation to methanol compared with other Au–CuO/CeO_2 samples. The 1 wt% Au–CuO/CeO_2 has a better ability to dissociatively adsorb hydrogen and enhance the number of oxygen vacancies, which leads to the highest methanol selectivity ($T = 240$ °C, $P = 3$ MPa, $S_{CH_3OH} = 29.6\%$). The in situ DRIFTS reveals that a dual site character of the Au–CuO/CeO_2 catalysts for CO_2 hydrogenation, with CO_2 being activated on sites of the CeO_2 support, then stepwise hydrogenation of (bi)carbonate to formate and methoxy, finally methanol.

Keywords CO_2 hydrogenation · Methanol selectivity · Gold addition · Hydrogen dissociation

1 Introduction

The atmospheric CO_2 accumulation, due to human activities such as burning fossil fuels, deforestation, land use change and cement production, has become a serious problem for our environment on account of global warming, climate change, ocean acidification and glaciers melting. Hydrogenation of CO_2 to methanol is an attractive and promising way to solve excess CO_2 emission and energy shortage problems [1]. Methanol is a both a clean energy source and a versatile chemical for several chemical processes.

Due to the high thermodynamic stability of CO_2, splitting of a C–O bond in the molecule is characterized by a high energy barrier. Thus, effective activation of CO_2 is a critical step in improving the overall reaction kinetics of the process. Apart from CO_2 activation, the number of active H atom is also a key parameter, which is necessary to promote hydrogenation of intermediate species [2].

Cu-supported catalysts have been widely used in methanol synthesis from CO_2 hydrogenation [3, 4]. Providing more active hydrogen atom can probably further improve catalytic activity of Cu-based catalysts. It has been reported that the addition of gold metal to Cu-based catalysts, which can dissociate hydrogen efficiently [5, 6]. Au NPs have out-standing efficiency in a broad range of catalytic reactions [7]. The smaller Au NPs have more interfacial sites and low-coordinated Au atoms, which are believed to be the active sites to boost the chemical activity [7–9]. The Au-containing catalysts may not always be active for hydrogenation. Because of its unique plasmon character, gold has been extensively used for the photocatalytic conversion of CO_2 [10, 11].

Compared to the traditional industrial $Cu/ZnO/Al_2O_3$ catalyst, which has been extensively characterized and studied, these Au catalysts are still barely understood. It has been found that the first subgroup B elements of the periodic table (such as Au and Cu) could produce strong interaction or form alloy with each other, which is the reason for more active on bimetallic Au–Cu catalyst compared to the individual Au and Cu catalysts [12]. It has shown that CeO_2 is an appropriate support to react with CO_2 due to its basic property [13]. Additionally, a synergy of the Au

Weiwei Wang and Desiree Wager Kimpouni Tongo have contributed equally to this work.

✉ Zhenping Qu
quzhenping@dlut.edu.cn

[1] Key Laboratory of Industrial Ecology and Environmental Engineering, School of Environmental Science and Technology, Dalian University of Technology, Dalian 116024, China

with copper to promote a direct and selective conversion of CO_2 into methanol has not been identified. In this regard, CeO_2-supported Au–CuO catalysts with different Au loading are employed to illustrate the role of Au in tuning CO_2 hydrogenation selectivity.

2 Experimental

2.1 Catalyst Preparation

In the first step, the reducible oxide support CeO_2 was prepared. The solution of precursor [$Ce(NO_3)_3{\cdot}6H_2O$] was continuously stirred and then co-precipitated using NaOH (0.2 mol/L) as a precipitant. The suspension was aged for 2 h. The resulting precipitate was obtained by filtration, washed with deionized water and ethanol for three times to remove the excess ions. Next, the samples were dried overnight at 80 °C in air and calcined at 500 °C for 4 h under air. Then the bimetallic Au–CuO/CeO_2 catalysts were prepared by co-impregnation method with a amount of $HAuCl_4$ (0.5, 1, 2 wt% Au) solution, $Cu(NO_3)_2{\cdot}3H_2O$ (10 wt%) solution and the CeO_2 support. After 30 min of ultrasonic, the obtained samples were dried and calcined at 400 °C for 4 h. The Au–CuO/CeO_2 catalysts with different Au contents were denoted x wt% Au–CuO/CeO_2 (x = 0.5, 1, 2 wt%).

2.2 Catalyst Characterization

XRD patterns of the calcined catalysts were recorded using a D/max 22,000. The scanning angle was adjusted from 20° to 80° at 2θ Bragg angle with a step size of 0.02° and a time/step of 11 s. This technique was used to examine crystallite phase composition and mean particle size. The mean crystallite size was calculated by Debye–Scherrer equation.

Raman spectra were recorded on a Renishaw equipment. Room-temperature Raman were excited at 532 nm, the exposure time was 2 s and the accumulation number was 20 times.

The surface properties of pre-reduced catalysts were obtained by X-ray photoelectron spectroscopy (XPS). XPS was performed on K-Alpha + with 5×10^{-9} mbar analysis chamber vacuum. Spectra were obtained for the C 1 *s*, O 1 *s*, Au 4*f*, Ce 3*d* and Cu 2*p* regions.

The reducibility property of the samples was investigated by TPR on a PCA-1200 chemical adsorption instrument. The catalysts were pretreated in a home-made U-shape quartz reactor under an N_2 flow. After this pretreatment, the catalysts were cooled to room temperature. A reducing gas of 10% (v/v) H_2 in He was then exposed into the reactor at a flow rate of 120 mL/min and the samples were heated up to 500 °C at a heating rate of 10 °C/min.

H_2/CO_2 temperature programmed desorption were operated on a mass spectrometer (OmniStar 320). Before the TPD analysis, all catalysts were reduced with H_2 (50 mL/min) at 300 °C for 3 h and went through the pretreatment under He at a rate of 60 mL/min at 310 °C for 0.5 h to clean the catalyst surface. After cooling to room temperature, the catalyst was saturated with a $V_{CO_2}/V_{He} = 1{:}3$ at room temperature for 0.5 h, followed by purging with He for 1 h to remove the physisorbed molecules. Afterwards, the TPD experiment was started in flowing He with a heating rate of 10 °C/min, and the desorbed CO_2 data was detected by mass spectrometer (OmniStar 320). H_2 temperature-programmed desorption (H_2-TPD) were performed as the same procedure as CO_2-TPD, and the difference is that the catalyst was saturated with $V_{H_2}/V_{He} = 3{:}1$.

The in situ DRIFTS measurements were done on a VERTEX equipment at the temperature of 240 °C and 3 MPa. The sample was placed in a ceramic crucible in an in situ DRIFTS cell fitted with ZnSe windows and connected to stainless steel gas lines. The in situ DRIFTS spectra were recorded with a resolution of 4 cm^{-1} and with an accumulation of 32 scans every 30 s during the temperature ramp. The IR data were analyzed by the OPUS software. The in situ DRIFTS spectra shown in this work were expressed in units of Kubelka–Munk. Similar to the reaction tests, the samples were also pretreated under H_2 atmosphere at 300 °C. Subsequently, the catalysts were cooled down to the reaction temperature. The procedures of in situ DRIFTS experiment were as follows: (1) exposing to CO_2/N_2 mixture gas (60 mL/min); (2) treating in a N_2 gas flow (60 mL/min); (3) changing to the reaction gas mixture CO_2/H_2 at a flow rate of 60 mL/min for CO_2 hydrogenation; (4) exposing to H_2/N_2 atmosphere.

2.3 Catalytic Activity

Activity measurements for CO_2 hydrogenation were carried out in a fixed bed reactor. 0.5 g of catalyst was placed in a stainless-steel tube reactor with diameter of 20 mm and length of 200 mm. Prior to the activity studies, the calcined catalyst was reduced at 300 °C for 3 h in pure H_2 at a rate of 5 °C /min. After reduction, CO_2 hydrogenation process was performed with a 1:3 molar ratio of $CO_2{:}H_2$, pressure of 3 MPa, temperature range between 200 and 300 °C. The activity test experiment keeps 2 h at each temperature. CO_2 and CO were quantitatively analyzed using gas chromatograph (GC) equipped with a thermal conductivity detector and Porapak-Q column (GC7890T), the target product CH_3OH was analyzed by using GC7900 equipped with flame ionization detector and a capillary column.

3 Results and Discussion

3.1 Physico-chemical Properties

To determine the crystalline phase compositions of catalyst, XRD is then carried out and the patterns are shown in Fig. 1. The reflection peaks associated with Au element (Au oxide species or metallic Au species) are not observed in the XRD pattern of x wt% Au/CuO–CeO_2 catalysts. The probable reason to explain is that the presence of the Au is in a form of highly dispersed nano-particles on the surface or the Au concentrations are below the detection limits. The diffraction peaks at 28.5°, 32.9°, 47.4°, 56.3°, 59.1°, 69.4°, 76.7°, and 78.9° are attributed to CeO_2 with a face-centered cubic fluorite structure, and those at 35.5° and 38.7° are well consistent with CuO of monoclinic structure [14]. Additionally, the peaks associated with CuO species become broaden after adding gold to the catalysts, it is indicated that adding gold is beneficial to disperse the copper species and reduce the size of CuO species.

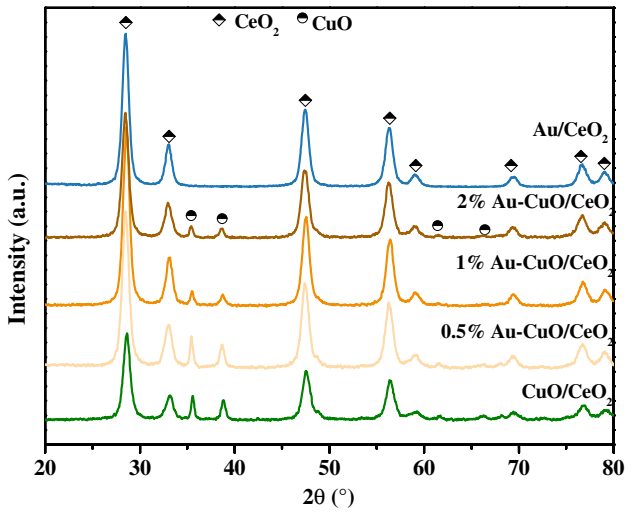

Fig. 1 XRD patterns of monometallic Au/CeO_2, CuO/CeO_2 and bimetallic Au–CuO/CeO_2 catalysts

As depicted in Fig. 2, it is widely known that pure CeO_2 sample presents a prominent peak at 464 cm^{-1} corresponding to F_{2g} Raman active mode in CeO_2 with fluorite-like structure [15], which can be viewed as a symmetric breathing mode of oxygen atoms surrounding cerium ions. For all the samples, the bands at 297 cm^{-1} and 632 cm^{-1} associated with oxygen vacancies appear [16]. The peak fitting for 632 cm^{-1} and 464 cm^{-1} is plotted in Fig. 2a, and the A_{632}/A_{464} value for Au/CeO_2 is the lowest (0.02). The value for CuO/CeO_2 (0.18) is much higher than that of Au/CeO_2. For the x wt% Au–CuO/CeO_2 samples, the A_{632}/A_{464} value increases compared with monometallic catalysts. The higher A_{632}/A_{464} value of 0.36 for 1 wt% Au–CuO/CeO_2 suggests the presence of larger number of oxygen vacancy sites, compared with the values of 0.23 and 0.25 for 0.5 wt% Au–CuO/CeO_2 and 2 wt% Au–CuO/CeO_2, respectively. The surface oxygen vacancies concentrations of all reduced samples are investigated by XPS. The changing trend of surface relative $Ce^{3+}/(Ce^{4+}+Ce^{3+})$ ratio is same to the variation of oxygen vacancies concentration (Table 2; Fig. 3b). The concentration of $Ce^{3+}/(Ce^{4+}+Ce^{3+})$ is in order: 1 wt% Au–CuO/CeO_2 (39.4%) > 0.5 wt% Au–CuO/CeO_2 (33.1%) > 2 wt% Au–CuO/CeO_2 (30.6%) > CuO/CeO_2 (32.1%) > Au/CeO_2 (23.4%). The transformation of Ce^{4+} to Ce^{3+} can create the charge imbalance and oxygen vacancy on the catalyst according to the charge compensation. Meanwhile the relative amount of the defect oxygen species (O_β) on the surface varies with the amount of the Au contents. 1 wt% Au–CuO/CeO_2 has the highest $O_\beta/(O_\alpha+O_\beta+O_\gamma)$ concentration.

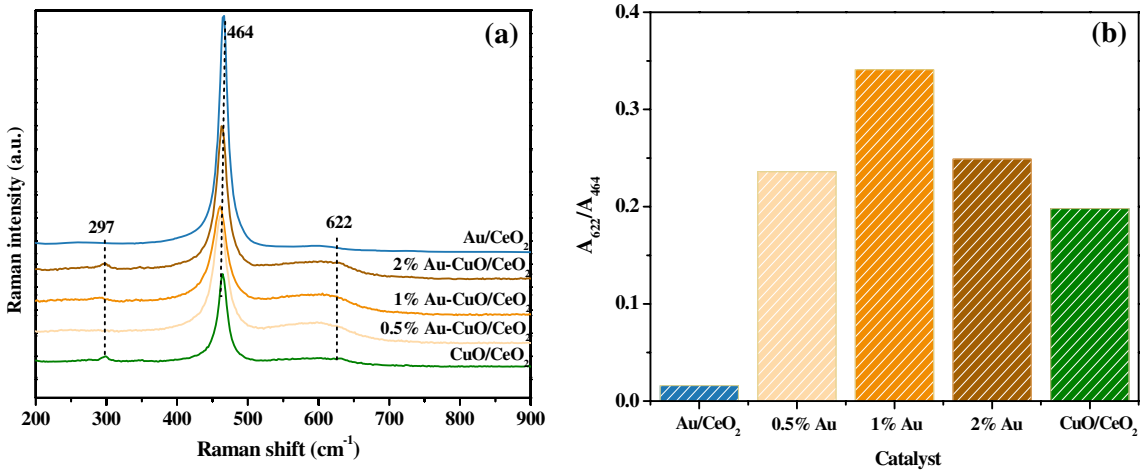

Fig. 2 **a** Raman spectra of different catalysts and **b** concentration of oxygen vacancies on the tested samples

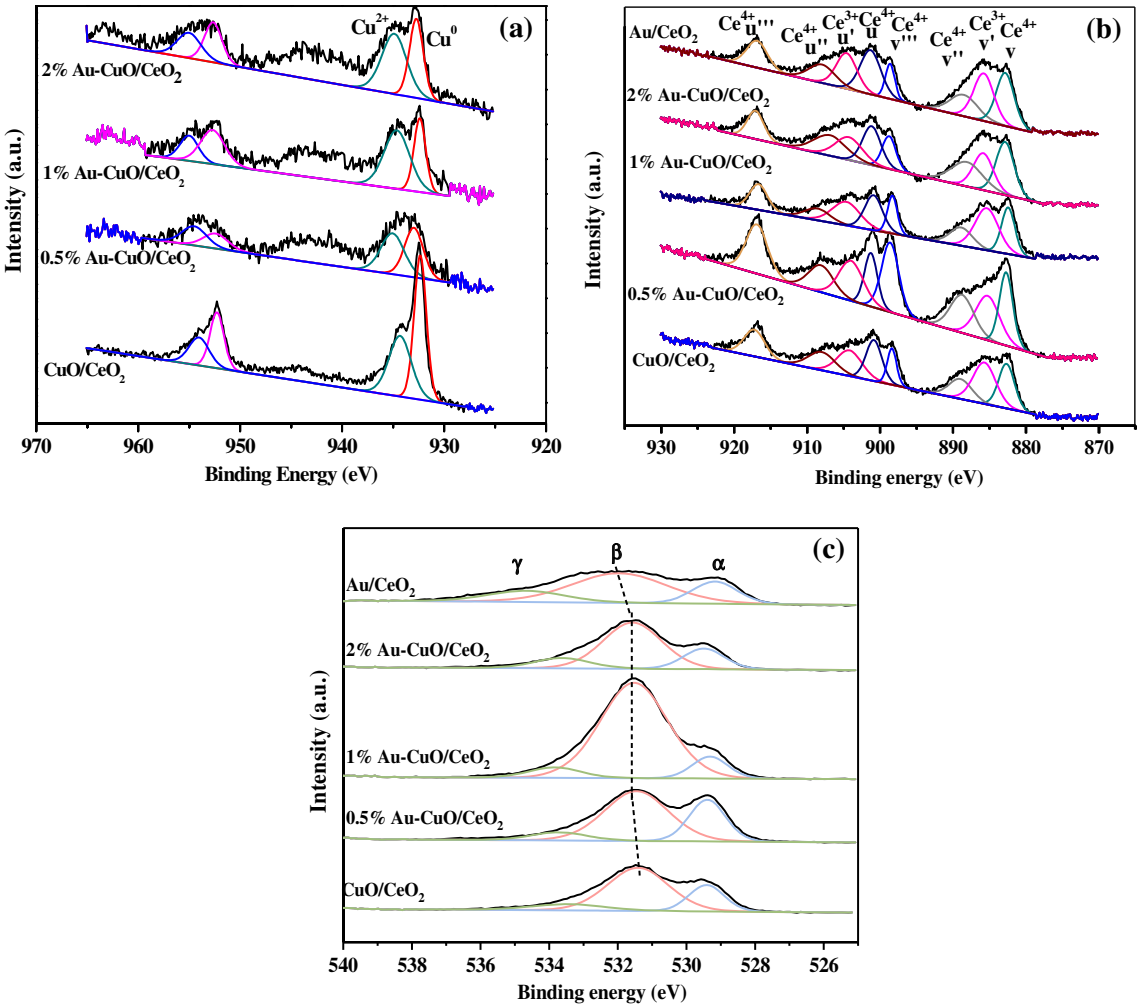

Fig. 3 XPS spectra of **a** Cu 2*p*, **b** Ce 3*d*, and **c** O 1*s* of the H_2-reduced catalysts

Above all, the trend of surface oxygen vacancies concentration is same to that of the bulk oxygen vacancies concentration. And 1 wt% Au–CuO/CeO_2 has the highest concentration in both reduced state and oxidized state.

Oxygen vacancies in a metal oxide support have been identified as one of the key components which can impact the chemical behavior of CO_2 [17]. It is found that adding gold also promotes the formation of oxygen vacancies, especially for 1 wt% Au–CuO/CeO_2 catalyst. The excess and insufficient gold content have a negative effect on the formation of defect oxygen, which may be associated with the different promotion ability of reduction of Ce^{4+} to Ce^{3+} for Au–CuO/CeO_2 samples with different gold contents [18].

The H_2-TPR profiles of the tested samples are shown in Fig. 4. The peak at the lower temperature of 215 °C for Au/CeO_2 is ascribed to the reduction of ceria surface oxygen and/or the reduction of partially oxidized gold species [19]. This peak is observed at much higher temperatures (> 550 °C) over pure CeO_2, implying that the addition of

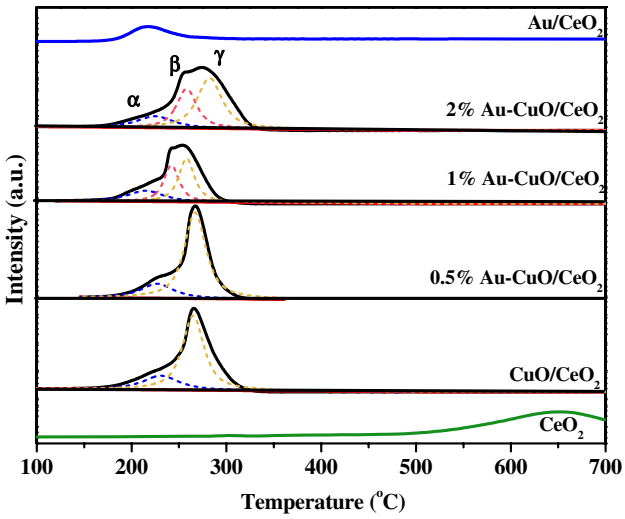

Fig. 4 H_2-TPR profiles of Au/CeO_2, CuO/CeO_2 and Au–CuO/CeO_2 catalysts

gold to CeO_2 facilitates the reduction of surface oxygen species. CuO/CeO_2 shows two reduction peaks, α peak (210–220 °C) is attributed to the reduction of small particle size of CuO species and/or the ceria surface oxygen, γ peak (255–265 °C) is attributed to large particle of CuO species [7]. The reduction temperature of $Au–CuO/CeO_2$ samples is lower than that of CuO/CeO_2 due to the addition of gold [20]. The 0.5 wt% $Au–CuO/CeO_2$ has almost the same CuO reduction peaks to those of CuO/CeO_2, because of the low concentration of gold. Differently, 1 wt% and 2 wt% $Au–CuO/CeO_2$ samples show three H_2 consumption peaks. Moreover it is found that more oxygen species could be reduced at lower temperatures on these both catalysts. Based on XRD result, CuO particle sizes of 1 wt% and 2 wt% $Au–CuO/CeO_2$ samples are smaller, hence, new reduction peak β should be due to the presence of middle particle size of CuO. In addition, a upward shift of the reduction peak from 240 to 258 °C is observed when gold content increases from 1 to 2 wt%, because the larger CuO particles are observed over 2 wt% $Au–CuO/CeO_2$ sample. The shift of binding energy of Cu $2p_{3/2}$ peak in all $Au–CuO/CeO_2$ samples is observed (Fig. 3a), which suggests that gold addition promotes the CuO reduction and then shifts the reduction temperature to lower. The addition of the gold weakens the Cu–O bond, enhancing the reducibility of CuO [21].

Apart from CO_2 activation, the supply of H adatoms is also important for the hydrogenation reaction in the methanol formation. Figure 5 shows the H_2-TPD profiles of H_2-reduced catalysts. No desorption peaks are observed over CeO_2. Au/CeO_2 has an extremely weak and broad desorption peak at around 150–300 °C, indicating that gold particles are responsible for dissociation of H_2 over Au/CeO_2. The CuO/CeO_2 catalyst displays two stronger desorption peaks. The

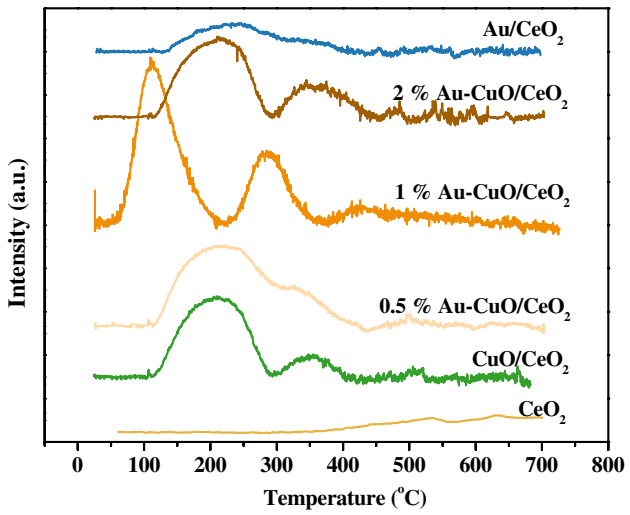

Fig. 5 H_2-TPD profiles of Au/CeO_2, CuO/CeO_2 and $Au–CuO/CeO_2$ catalysts

former desorption is attributed to the desorption of atomic hydrogen, and the high-temperature desorption peak presents the desorption of strongly adsorbed hydrogen on the bulk of metal particles [20]. It is demonstrated that monometallic gold and copper catalysts are likely to be responsible for H_2 adsorption during CO_2 hydrogenation. The spectra of 0.5 wt% $Au–CuO/CeO_2$ sample is almost same to that of CuO/CeO_2 because of low Au concentration. For 1 wt% $Au–CuO/CeO_2$ sample, the H_2 desorption temperature is lower and amount of H_2 desorption is larger. However further increase the amount of gold, 2 wt% $Au–CuO/CeO_2$ sample present a higher H_2 desorption temperature and smaller H_2 desorption compared to 1 wt% $Au–CuO/CeO_2$ sample, which might be result of larger CuO particles.

The Cu 2*p* spectra for the reduced samples are presented in Fig. 3a. For all samples, a main peak around 932.4 eV shows that the copper species are mainly in Cu^0 state after reduction. Cu $2p_{3/2}$ component at 933.7 eV and the shake-up peak indicate the presence of Cu^{2+} ions [22]. The ratio of $Cu^0/(Cu^{2+}+Cu^0)$ over all samples is almost the same (46.4–47.8%). Generally, it is acknowledged that Cu^0 is responsible for dissociation of H_2. Based on the XRD and XPS results, the dispersion and the number of Cu^0 is almost the same among all the samples. However, it has shown the samples have different H_2 adsorption ability, which is probably due to the presence of Au.

The characteristic peaks of Au^0 and Au^+ species over 1 wt% $Au–CuO/CeO_2$ are located at 83.8 eV and 85.7 eV in Au $4f_{7/2}$, while at 88.4 eV and 89.6 eV in Au $4f_{5/2}$. It can be observed that the gold species on the surface of $Au–CuO/CeO_2$ samples is mainly Au^+, with small amounts of Au^0. When the H_2 molecule interacts with Au^+, the anti-bonding states will be less filled compared with metallic Au [14]. This will stabilize the binding between H_2 and Au^+, facilitating the splitting of the molecule. In this work, we configure that Au interaction with the Cu enables the ability to supply H adatoms to hydrogenate CO_2. It has been demonstrated that the hydrogen spillover weakens and the amount of H_2 consumed decreases due to inappropriate gold–copper interaction (too weak or strong), over 0.5 wt% and 2 wt% samples. Differently, the interaction between gold and copper over 1 wt% $Au–CuO/CeO_2$ leads to the superior hydrogen spillover, therefore exhibiting better desorption properties.

3.2 Catalytic Activity

The catalytic performance results of the catalysts are shown in Table 1. CuO/CeO_2 exhibits low catalytic performance toward methanol synthesis from CO_2 hydrogenation. Specifically the CO_2 conversion of which is as low as 3.8–9.6% from 200 to 300 °C. The methanol selectivity increases from 8.6 to 17.9% at 200–240 °C, then decreases to 4.3% at 300 °C. Au/CeO_2 shows relatively high CO_2 conversion

Table 1 XPS data measured for Au/CeO_2, Cu/CeO_2 and $Au–CuO/CeO_2$ catalysts

Catalyst	$Ce^{3+}/(Ce^{3+}+Ce^{4+})$ (%)	$O_\beta/(O_\alpha+O_\beta+O_\gamma)$ (%)	$Cu^0/(Cu^0+Cu^{2+})$ (%)
CuO/CeO_2	32.1	65.4	46.7
0.5% $Au–CuO/CeO_2$	33.1	67.8	47.4
1% $Au–CuO/CeO_2$	42.4	82.9	47.8
2% $Au–CuO/CeO_2$	30.6	66.7	46.4
Au/CeO_2	23.4	59.2	NA

(6.8–12.7% at 200–300 °C), but it favors the formation of CO rather than methanol. The methanol selectivity of Au/CeO_2 keeps decreasing from 21.8 to 0.6% during whole process. Adding 1 wt% gold increases CO_2 conversion (6.3–10.1% at 200–300 °C). The 1 wt% $Au–CuO/CeO_2$ catalyst exhibits the highest methanol selectivity (29.6%) at 240 °C. The improvement of methanol selectivity over 1 wt% $Au–CuO/CeO_2$ is even higher than that of CO_2 conversion, especially for higher reaction temperature (≥ 240 °C). However methanol selectivity is found to drop with further addition of gold (2 wt%).

A comparison of catalytic activity on Cu/Au-based catalysts for CO_2 hydrogenation to methanol is summarized in Table 2. The monometallic Au-based catalysts with equivalent gold loading (1.1 wt%) to our work, which shows lower CO_2 conversion and CH_3OH selectivity compared with 1 wt% $Au–CuO/CeO_2$ in our work [23, 24]. Though the monometallic Cu-based catalysts with higher copper contents, the catalytic performance of these samples is still lower than that of 1 wt% $Au–CuO/CeO_2$ [25–27]. For bimetallic Au–Cu samples studied by other researchers [28], CO_2 conversion of these samples is higher than that of 1 wt% $Au–CuO/CeO_2$, however, CH_3OH selectivity of these samples is much lower.

The 1 wt% $Au–CuO/CeO_2$ shows the highest methanol selectivity among all samples. The CuO particle size of monometallic CuO/CeO_2 and bimetallic $Au–CuO/CeO_2$ samples is almost similar (22–26 nm), which indicates that particle size has little influence on catalytic performance. It is speculated that the excellent catalytic performance of 1 wt% $Au–CuO/CeO_2$ sample can be attributed to larger amounts of oxygen vacancies and active H atoms.

3.3 In Situ DRIFTS Study

3.3.1 High Pressure In Situ DRIFTS of CO_2 Adsorption

The 1 wt% $Au–CuO/CeO_2$ sample with best catalytic performance is chosen as a representative one to illuminate the effect of Au addition on CO_2 adsorption over 1 wt% $Au–CuO/CeO_2$ sample. After CO_2 adsorption, the methoxy species (1016, 1048 and 1078 cm^{-1}) and bicarbonates (1240, 1286, 1646 and 1689 cm^{-1}) are observed over CeO_2 sample (Fig. S1a). For Au/CeO_2 sample, the main adsorption species still are methoxy and bicarbonate species, additionally, one weak peak associated with formate species is detected (Fig. S1b). However, for CuO/CeO_2 sample, only methoxy species are the main adsorption ones, indicating that the copper species on the CeO_2 has an effect on adsorption of CO_2 (Fig. S1c). Muttaqien et al. has demonstrated that pure copper species have ability to adsorb CO_2 and the properties of copper species have an influence in CO_2 adsorption capacity [29]. As is shown in Fig. S1d, the CO_2 adsorption species on 0.5 wt% $Au–CuO/CeO_2$ are similar to those of on CuO/CeO_2. The low Au content has a little effect on CO_2 adsorption. Figure 6 shows the spectra of CO_2 adsorption ranging from 1 to 30 min over 1 wt% $Au–CuO/CeO_2$ catalyst. The adsorption of CO_2 on 1 wt% $Au–CuO/CeO_2$ produces methoxy (1016, 1048 and 1078 cm^{-1}), bicarbonates (1240, 1286, 1646 and 1689 cm^{-1}) and carbonate species (1438 and 1521 cm^{-1}) [30]. The higher concentration and more types of adsorption species are observed on 1 wt% $Au–CuO/CeO_2$ catalyst. Hence, the addition of 1 wt% Au to CuO/CeO_2 promotes CO_2 adsorption due to the formation of the largest number of oxygen vacancies and excellent copper species properties. As adding 2 wt% Au to CuO/CeO_2, the type and concentration of adsorption species are becoming smaller (Table 3).

Combining with CO_2-TPD result (Fig. S3), pure CeO_2 only shows CO_2 desorption peaks ranging from 50 to 200 °C, which is assigned to weakly and moderately basic sites [31]. Additionally, a lager desorption peak at around 400 °C is observed on CuO/CeO_2 and 1 wt% $Au–CuO/CeO_2$ samples, which probably comes from the decomposition of carbonate species. As is confirmed by the result obtained from in situ DRIFTS of CO_2 adsorption (Figs. 6, S1), carbonates species are only detected on these two samples. Hence, it is reasonable to speculate that weakly and moderately basic sites are active sites for CO_2 adsorption and activation during CO_2 hydrogenation to methanol over $Au–CuO/CeO_2$ samples. Because 1 wt% $Au–CuO/CeO_2$ with a higher density of basic sites readily activates CO_2 and therefore it is reasonable to speculate that the hydrogenation activity is governed by the adsorption and dissociation of H_2.

3.3.2 High Pressure In Situ DRIFTS of CO_2 Hydrogenation

The in situ DRIFT spectra of 1 wt% $Au–CuO/CeO_2$ catalyst under CO_2+H_2 is displayed in Fig. 7. Since no peaks corresponding to methanol are observed. The support CeO_2 itself is not active for CO_2 hydrogenation to methanol. These results indicate that the presence of active metal is necessary for the CO_2 hydrogenation to methanol [32]. Neither Au/CeO_2 nor CuO/CeO_2 shows good methanol selectivity. Gold is demonstrated to be more selective and active for the

Table 2 The catalytic activity of Au–CuO/CeO_2 catalysts for CO_2 hydrogenation to methanol

Catalyst	200 °C X_{CO_2}	200 °C S_{CH_3OH}	200 °C S_{CO} (%)	220 °C X_{CO_2}	220 °C S_{CH_3OH}	220 °C S_{CO} (%)	240 °C X_{CO_2}	240 °C S_{CH_3OH}	240 °C S_{CO} (%)	260 °C X_{CO_2}	260 °C S_{CH_3OH}	260 °C S_{CO} (%)	280 °C X_{CO_2}	280 °C S_{CH_3OH}	280 °C S_{CO} (%)	300 °C X_{CO_2}	300 °C S_{CH_3OH}	300 °C S_{CO} (%)
CuO/CeO_2	3.8	8.6	0	5.1	12.1	10.6	5.2	17.8	13.5	5.4	11.4	24.1	5.9	3.9	41.6	6.9	4.3	52.9
Au/CeO_2	6.8	21.8	0	6.5	18.5	9.4	7.3	9.1	3.18	8.5	4.3	4.66	10.0	1.4	3.01	12.7	0.6	55.1
1 wt% Au	**6.3**	**11.4**	**0**	**6.1**	**28.0**	**0**	**6.7**	**29.5**	**7.4**	**7.1**	**20.5**	**14.2**	**8.7**	**26.1**	**9.47**	**10.1**	**11.2**	**37.3**
0.5 wt% Au	1.9	18.1	7.6	3.3	12.6	12.1	3.1	8.0	11.7	3.3	4.0	21.7	4.5	1.9	40.8	4.6	0.7	55.4
2 wt% Au	4.8	9.7	0	5.1	21.2	0	5.2	21.6	9.4	5.4	18.9	18.7	5.9	14.1	33.4	6.9	8.9	50.7

Bold values indicate the best catalytic performance compared with other samples

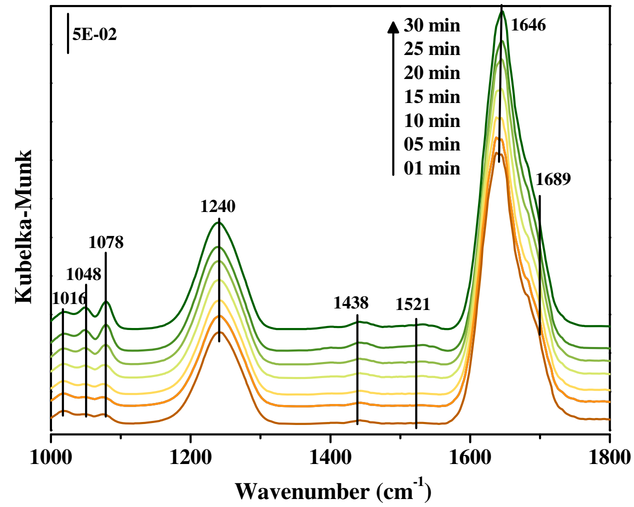

Fig. 6 In situ DRIFT spectra of CO_2 adsorption over 1% Au–CuO/CeO_2 catalysts under 240 °C and 3 MPa

formation of CO/CH_4 rather than CH_3OH product in CO_2 hydrogenation reaction [33]. For a series of Au–CuO/CeO_2 samples, the type and concentration of intermediate species on 0.5 wt% Au–CuO/CeO_2 is almost identical to those of on CuO/CeO_2 sample (Fig. S4d). For 2 wt% Au–CuO/CeO_2, only a small concentration of methanol is observed (Fig. S4e). The interaction between gold and copper of high/low gold loading catalyst is both unfavorable for providing active H* species.

Differently, compared to other samples, the intensities of methoxy (1078 and 1498 cm^{-1}) and formate (1390 and 2703 cm^{-1}) on 1 wt% Au–CuO/CeO_2 become stronger, suggesting an improvement of H_2 dissociation. And a larger number of methanol is detected on 1 wt% Au–CuO/CeO_2. Evidently, the interaction between gold and copper over 1 wt% Au sample leads to a remarkable enhancement of methanol selectivity, while the improvement is very little on their single counterparts. It is reported that the hydrogen spillover is beneficial to enhance methanol formation rate, resulting in higher methanol selectivity [34]. It has shown that the superior methanol selectivity of CuO–ZnO–ZrO_2–GO is attributed to a promotional effect of GO nanosheet serving as a bridge between mixed metal oxides which enhances a hydrogen spillover from the copper surface [35]. The hydrogen spillover improves methanol yield over Au/Cu–Zn–Al catalyst for methanol synthesis from CO_2 [28]. Thus it is reasonable to suggest that the fine interaction between Au and Cu promotes the hydrogen spillover over 1 wt% Au–CuO/CeO_2, resulting in higher methanol selectivity.

It is known that the reaction temperature also plays a significant role in the evolution of intermediate species, resulting in different catalytic performance of CO_2 hydrogenation to methanol. Figure 8 shows in situ DRIFT spectra

Table 3 The CO_2 conversion and CH_3OH selectivity on Au, Cu-based catalysts for CO_2 hydrogenation to methanol

Catalyst	H_2:CO_2 ratio	Temperature (°C)	Cu/Au content	Pressure (MPa)	CO_2 conversion (%)	CH_3OH selectivity (%)	References
Au–CuO/CeO_2	3:1	240	Au 1 wt% Cu 10 wt%	3	6.7	29.6	This work
Au–CuO/SBA-15	3:1	250	Au 3 wt% Cu 24 wt%	3	24	13.4	[5]
Au/Al_2O_3	3:1	240	Au 1.1 wt%	0.5	3.7	0.4	[16]
Au/ZrO_2	3:1	240	Au 1.1 wt%	0.5	9.3	3.4	[16]
Au/ZnO	3:1	240	Au 1.1 wt%	0.5	0.4	50.6	[16]
Au/ZnO/ZrO_2	3:1	220	Au 62.5 wt%	8	1.5	100	[17]
CuO/ZrO_2	3:1	220	Cu 32 wt%	3	4.2	53.9	[18]
CuO/TiO_2	3:1	220	Cu 10 wt%	3	0.19	29.8	[19]
CuO/ZnO	3:1	250	Cu 10 wt%	5	11.7	36.1	[20]
Au/Cu–Zn–Al	6:1	240	Au 1 wt% Cu 38 wt%	4	16	5	[21]

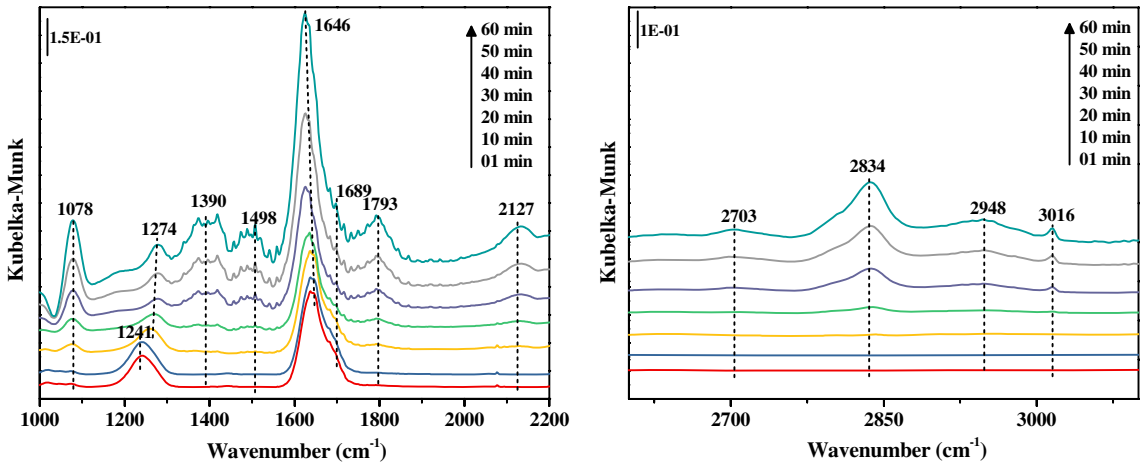

Fig. 7 In situ DRIFT spectra of CO_2+H_2 over 1% Au–CuO/CeO_2 catalysts at 1000–2200 cm^{-1} and 2600–3100 cm^{-1} under 240 °C and 3 MPa

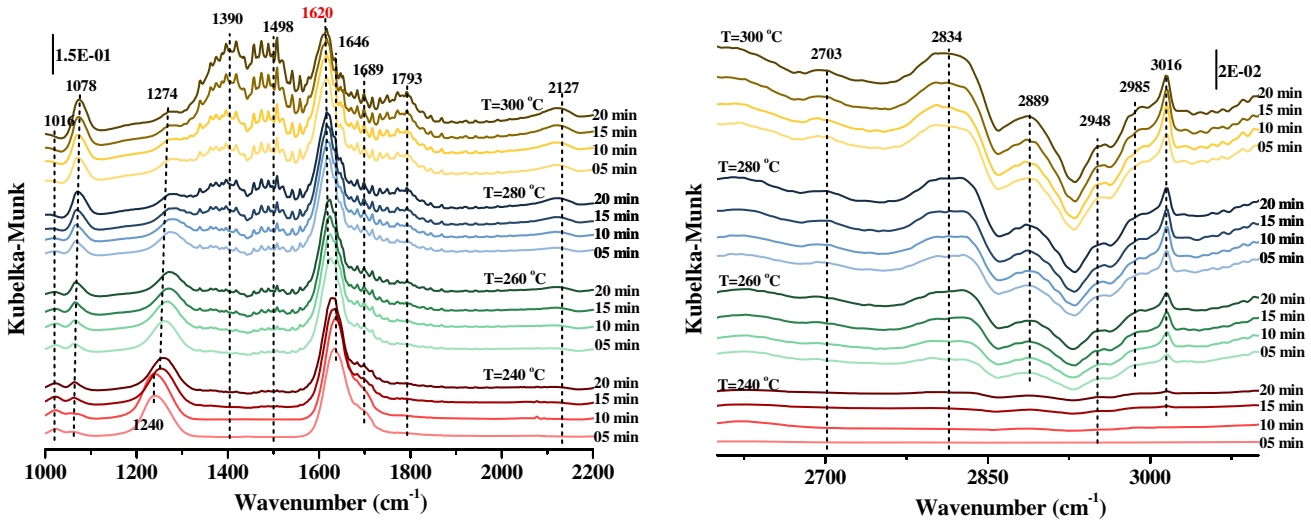

Fig. 8 In situ DRIFT spectra of CO_2+H_2 over 1% Au–CuO/CeO_2 between 240 and 300 °C at 1000–2200 cm^{-1} and 2600–3100 cm^{-1} under 240 °C and 3 MPa

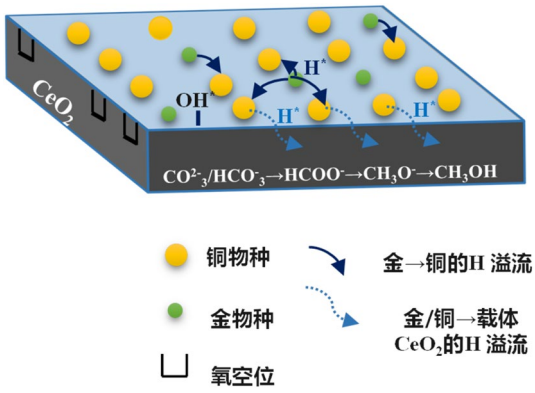

Scheme 1 Possible reaction pathway of CO_2 hydrogenation to methanol over 1% Au–CuO/CeO_2 sample

of CO_2 hydrogenation over 1 wt% Au–CuO/CeO_2 from 240 to 300 °C. The peaks assigned to bicarbonates (1240, 1274, 1646, 1689 cm^{-1}) decrease from 240 to 300 °C, simultaneously, the intensities of methoxy (1016, 1078, 1498 cm^{-1}), formate (1390, 2703 cm^{-1}) intermediates start to increase 240 °C to 300 °C. Additionally, methanol (2834 and 2948 cm^{-1}) and by-products CO (2127 cm^{-1}) as well as methane (3016 cm^{-1}) increase at 240–300 °C. Obviously, these observations illustrate that bicarbonates adsorbed on CeO_2 are firstly hydrogenated into formate, then methoxy and finally methanol, as is shown in Scheme 1. The findings proposed in the work would be helpful for designing complex catalysts with multiple active components.

4 Conclusions

This work investigates the effect of Au addition on catalytic performance of Au–CuO/CeO_2 catalysts for CO_2 hydrogenation to methanol. Tuning Au loading can affect the formation and evolution of the surface species, therefore controlling the catalytic performance. The 1 wt% Au–CuO/CeO_2 is able to activate both H_2 and CO_2 for the efficient production of methanol. Additionally, in situ DRIFT experiments suggest the formate pathway for the reaction mechanism on 1 wt% Au–CuO/CeO_2, and CO_2 molecular firstly is adsorbed and activated on CeO_2 forming (bi)carbonates, and then formate and methoxy species, finally methanol.

Supplementary Information The online version contains supplementary material available at https://doi.org/10.1007/s11244-021-01414-3.

Acknowledgements This work was financially supported by the National Nature Science Foundation of China (21876019), Fundamental Research Funds for the Central Universities (DUT19LAB10), Dalian Science and Technology Innovation Fund (2019J12SN74) and the Fund of the State Key Laboratory of Catalysis in DICP (N-18-08).

Author Contributions WW: Conceptualization, Methodology, Formal analysis, Data curation, Investigation, Writing-Original draft preparation. DWKT: Methodology, Formal analysis, Data curation, Investigation, Writing-Original draft preparation. LS: Visualization, Investigation, Software, Methodology. ZQ: Supervision, Funding acquisition, Project administration, Resources Validation, Conceptualization, Writing-Reviewing and Editing.

Compliance with Ethical Standards

Conflict of interest There is no conflict of interest when submitting this manuscript, and all authors have approved the publication of the manuscript. And the authors declare that they have no known competing financial interests or personal relationships that could have appeared to influence the work reported in this paper.

Ethical Approval I would like to state on behalf of my co-authors that the work described is the original study, has not been published before, and has not been considered for publication elsewhere. All the authors listed have approved the accompanying manuscript while being considered by Topics in Catalysis.

References

1. Roy S, Cherevotan A, Peter SC (2018) Thermochemical CO_2 hydrogenation to single carbon products: scientific and technological challenges. ACS Energy Lett 3:1938–1966
2. Yang CS, Pei CL, Luo R et al (2020) Strong electronic oxide-support interaction over In_2O_3/ZrO_2 for highly selective CO_2 hydrogenation to methanol. J Am Chem Soc 46:19523–19531
3. Din IU, Shaharun MS, Naeem A et al (2019) Revalorization of CO_2 for methanol production via ZnO promoted carbon nanofibers based Cu–ZrO_2 catalytic hydrogenation. J Energy Chem 39:68–76
4. Din IU, Alotaibi MA, Abdulrahman IA (2020) Green synthesis of methanol over zeolite based Cu nano-catalysts, effect of Mg promoter. Sustain Chem Pharm 16:100264
5. Bracey CL, Ellis PR, Hutchings GJ (2009) Application of copper–gold alloys in catalysis: current status and future perspectives. Chem Soc Rev 8:2231–2243
6. Martin O, Mondelli C, Curulla-Ferre D (2015) Zinc-rich copper catalysts promoted by gold for methanol synthesis. ACS Catal 5:5607–5616
7. Reina TR, Ivanova S, Centeno MA (2016) The role of Au, Cu and CeO_2 and their interactions for an enhanced WGS performance. Appl Catal B 187:98–107
8. Campbell CT (2004) The active site in nanoparticle gold catalysis. Science 5694:234–235
9. Sankar M, He Q, Engel RV (2020) Role of the support in gold-containing nanoparticles as heterogeneous catalysts. Chem Rev 120:3890–3938
10. Laszlo B, Baan K, Varga E (2016) Photo-induced reactions in the CO_2–methane system on titanate nanotubes modified with Au and Rh nanoparticles. Appl Catal B 199:473–484
11. Xue HR, Wang T, Gong H (2018) Constructing ordered three-dimensional TiO_2 channels for enhanced visible-light photocatalytic performance in CO_2 conversion induced by Au nanoparticles. Chem Asian J 5:577–583
12. Li Y, Na W, Wang H et al (2017) Hydrogenation of CO_2 to methanol over Au–CuO/SBA15 catalyst. J Porous Mater 24:591–599
13. Zhu JD, Su YQ, Chai JC et al (2020) Mechanism and nature of active sites for methanol synthesis from CO/CO_2 on Cu/CeO_2. ACS Catal 19:11532–11544

14. Jing GJ, Zhang L, Ma YR et al (2019) Comparison of Au–Ce and Au–Cu interaction over Au/CeO_2–CuO catalysts for preferential CO oxidation. CrystEngComm 21:363
15. Jeon S, Ham H, Suh Y et al (2015) Raman scattering study of cubic–tetragonal phase transition in $Zr_{1-x}Ce_xO_2$ solid solution. RSC Adv 5:54806–54815
16. Reddy BM, Khan A, Lakshmanan P et al (2005) Structural characterization of nanosized CeO_2–SiO_2, CeO_2–TiO_2, and CeO_2–ZrO_2 catalysts by XRD, Raman, and HRTEM techniques. J Phys Chem B 8:3355–3363
17. Ye J, Liu C, Mei D et al (2013) Active oxygen vacancy site for methanol synthesis from CO_2 hydrogenation on In_2O_3(110): a DFT study. ACS Catal 3:1296–1306
18. Liao X, Chu W, Dai X et al (2013) Bimetallic Au–Cu supported on ceria for PROX reaction: effects of Cu/Au atomic ratios and thermal pretreatments. Appl Catal B 142–143:25–37
19. Vourros A, Garagounis I, Kyriakou V et al (2017) Carbon dioxide hydrogenation over supported Au nanoparticles: effect of the support. J CO2 Util 19:247–256
20. Gamboa-Rosales NK, Ayastuy JL, Gonzalez-Marcos MP et al (2012) Oxygen-enhanced water gas shift over ceria-supported Au–Cu bimetallic catalysts prepared by wet impregnation and deposition-precipitation. Int J Hydrog Energy 37:7005–7016
21. Pongstabodee S, Monyanon S, Luengnaruemitchai A (2012) Hydrogen production via methanol steam reforming over Au/CuO, Au/CeO_2, and Au/CuO–CeO_2 catalysts prepared by deposition-precipitation. J Ind Eng Chem 18:1272–1279
22. An B, Zhang J, Cheng K et al (2017) Confinement of ultrasmall Cu/ZnO_x nanoparticles in metal–organic frameworks for selective methanol synthesis from catalytic hydrogenation of CO_2. J Am Chem Soc 139:3834–3840
23. Nevanperä TK, Ojala S, Laitinen T et al (2019) Catalytic oxidation of dimethyl disulfide over bimetallic Cu–Au and Pt–Au catalysts supported on γ-Al_2O_3, CeO_2, and CeO_2–Al_2O_3. Catalysts 9:603
24. Tan Q, Shi Z, Wu D (2018) CO_2 Hydrogenation to methanol over a highly active Cu–Ni/CeO_2-nanotube catalyst. Ind Eng Chem Res 57:10148–10158
25. Patil P, Nakate UT, Harish K et al (2020) Au sensitized La–CeO_2 catalyst coated ceramics monoliths for toluene catalysis application. Mater Chem Phys 240:12269
26. Piqueras CM, Puccia V, Vega DA et al (2016) Selective hydrogenation of cinnamaldehyde in supercritical CO_2 over Me–CeO_2 (Me = Cu, Pt, Au): insight of the role of Me–Ce interaction. Appl Catal B 185:265–271
27. Pongstabodee S, Monyanon S, Luengnaruemitchai A (2012) Hydrogen production via methanol steam reforming over Au/CuO, Au/CeO_2, and Au/CuO–CeO_2 catalysts prepared by deposition–precipitation. J Ind Eng Chem 18:1272–1279
28. Wang G, Chen L, Sun Y et al (2015) Carbon dioxide hydrogenation to methanol over Cu/ZrO_2/CNTs: effect of carbon surface chemistry. RSC Adv 5:45320–45330
29. Muttaqien F, Hamamoto YJ, Hamada I et al (2017) CO_2 adsorption on the copper surfaces: van der Waals density functional and TPD studies. J Chem Phys 147:094702
30. Fisher IA, Bell AT (1997) *In-situ* infrared study of methanol synthesis from H_2/CO_2 over Cu/SiO_2 and Cu/ZrO_2/SiO_2. J Catal 172:222–237
31. Sloczynski J, Grabowski R, Kozlowska A et al (2004) Catalytic activity of the M/(3ZnO–ZrO_2) system (M = Cu, Ag, Au) in the hydrogenation of CO_2 to methanol. Appl Catal A 278:11
32. Wang YH, Gao WG, Wang H et al (2017) Structure–activity relationships of Cu–ZrO_2 catalysts for CO_2 hydrogenation to methanol: interaction effects and reaction mechanism. RSC Adv 7:8709
33. Liu X, Guo Q, Guo D et al (2016) Methanol synthesis from CO_2 hydrogenation over copper catalysts supported on MgO-modified TiO_2. J Mol Catal A 425:86–93
34. Fujitani T, Saito M, Kanai Y et al (1995) Development of an active Ga_2O_3 supported palladium catalyst for the synthesis of methanol from carbon dioxide and hydrogen. Appl Catal A 125:199–202
35. Pasupulety N, Driss H, Alhamed YA et al (2015) Studies on Au/Cu–Zn–Al catalyst for methanol synthesis from CO_2. Appl Catal A 504:308–318